Structural and dynamic heterogeneity in the amorphous phase of Poly(L,L-lactide) confined at the nanoscale by the coextrusion process

Samira Fernandes Nassar, Sandra Domenek, Alain Guinault, Gregory Stoclet, Nicolas Delpouve, Cyrille Sollogoub

Structural and dynamic heterogeneity in the amorphous phase of Poly(L,L-lactide) confined at the nanoscale by co-extrusion process

Samira Fernandes Nassar[1], Sandra Domenek[1], Alain Guinault[2], Gregory Stoclet[3], Nicolas Delpouve[4], Cyrille Sollogoub[2*]

1: UMR Ingénierie Procédés Aliments, AgroParisTech, INRA, Université Paris-Saclay, 1 avenue des Olympiades, F-91300 Massy, France

2: PIMM, Arts et Métiers-ParisTech/CNAM/CNRS UMR 8006, 151 bd de l'Hôpital, 75013 Paris, France

3: UMR CNRS 8207, Unité Matériaux et Transformations, Université Lille1 Sciences et Technologies, Bâtiment C6, Université de Lille Nord de France, 59655 Villeneuve d'Ascq, France

4: Normandie Univ, UNIROUEN Normandie, INSA Rouen, CNRS, GPM, 76000 Rouen, France

Corresponding author: cyrille.sollogoub@lecnam.net

Key words: PLLA, poly(lactic acid), confinement, RAF, rigid amorphous fraction, CRR

Abstract

Multi-nanolayered Polystyrene/Poly(L,L-lactide) (PS/PLLA) films were obtained by the layer-multiplying co-extrusion process, with an individual PLLA layer thickness as thin as 20 nm. The confinement of the amorphous PLLA induced a change in the molecular mobility, evidenced by a drop of the Cooperative Rearranging Region (CRR) size at the glass transition. The annealing of confined PLLA layers revealed slower crystallization kinetics and two-dimensional crystalline growth geometry. Furthermore, the annealing of PLLA in confined layers allowed a decoupling between the amorphous and crystalline phase, evidenced by the absence of a Rigid Amorphous Fraction (RAF). As a consequence, the dynamic heterogeneity at the glass transition remained unaffected by the annealing procedure. In bulk polymers, where the level of coupling between amorphous and crystals is high, the glass transition temperature increased significantly whereas the CRR size fell. It is deduced that the glass transition dynamics in semi-crystalline polymers is strongly related to the mobility landscape at the interface with crystals.

Reference: Fernandes Nassar S, Domenek S, Guinault A, Stoclet G, Delpouve N, Sollogoub C (2018) Structural and Dynamic Heterogeneity in the Amorphous Phase of Poly(L,L-lactide) Confined at the Nanoscale by the Coextrusion Process. Macromolecules 51 (1):128-136. doi:10.1021/acs.macromol.7b02188

1. Introduction

Confining a polymer to a scale comparable to its different characteristic lengths (gyration radius or dimensions of the crystalline structure for example) leads to strong deviations of the structural and dynamical properties from the bulk. Since the pioneering work of Jackson and McKenna [1] on T_g deflection of organic liquids in nanopores, many studies [2-4] have discussed the effect of geometrical confinement on the molecular mobility and the glass transition temperature deviations of amorphous polymers. Similarly, crystallization under confinement has been shown to generate distinct features from bulk crystallization, possibly leading to a great variety of crystalline morphologies, inducing unique preferential orientations [5, 6]. In the aim of searching for finite size effects, a variety of experimental systems and geometries has been proposed to confine both amorphous and semi-crystalline polymers: droplet dispersions [7], thin films [8] or nano-layers [9], polymers infiltrated in inorganic nanotemplates (nanocylinders, nanolayers, nanospheres and nanopores) [10, 11], and self-assembled block copolymers [12]. Confinement can also be present, probably in a less regular and controllable way, in material systems like polymer blends [13], nanocomposites [14] and semi-crystalline polymers [15].

In semi-crystalline polymers, the amorphous phase appears to be constrained by the crystalline lamellae. This constraint is the consequence of both a geometrical confinement and a covalent coupling between the lamellae and the non-crystalline regions through tie molecules. When this coupling is strong enough, a separate phase of nanometric size can be produced at the interface between the two phases. A three phase model is therefore necessary to fully describe the semi-crystalline structure, in which the amorphous phase is split into two differently mobile fractions: the rigid amorphous fraction (RAF) as opposed to the mobile amorphous fraction (MAF) [16, 17]. While the latter relaxes at the glass transition, the former devitrifies at higher temperatures than T_g. The exact temperature at which the RAF vitrifies and devitrifies has been extensively studied and seems to mainly depend on the type of polymer investigated [17]. Moreover, the presence of RAF, having its own specific properties, not only modifies the mobility of the amorphous phase but may impact also the macroscopic properties, especially mechanical [18, 19] and gas barrier properties [20, 21]. Therefore, the RAF must be taken into account and thoroughly characterized in order to propose a complete understanding of the structure – property relationships in semi-crystalline polymers.

Polylactide (PLA) is a polyester with slow crystallization rate, different polymorphic forms [22] and a tendency to form RAF [23-28]. The RAF formation in PLA has been extensively studied and clearly correlated with the crystal growth [25, 27, 29]: at low crystallization temperature (near the glass transition) polymer chains have low mobility, which hampers the organization of the polymeric segments in ordered crystal structures. This causes coupling of the crystalline and amorphous phase by tie chains which can be observed by the existence of the RAF [24-26, 28, 29]. The RAF at low temperatures develops in parallel with the crystals, whereas for higher crystallization temperatures (near melting), the RAF appears at long crystallization time simultaneously with the secondary crystallization, occurring after spherulite impingement. Because of the existence of extensive knowledge, PLA is a good candidate for creating semi-crystalline systems with tailored crystalline morphology and controlled RAF in order to study the impact of the induced geometrical confinement on the amorphous phase dynamics. In this aim, different theoretical approaches and experimental techniques (differential scanning calorimetry, dielectric relaxation spectroscopy, and dynamic mechanical analysis) have been used and have sometimes led to contradictory results. While Mijovic et al. [30] did not observe any change in the glass transition dynamics upon crystallization, Fritz et al. [31] measured a significant T_g decrease when PLA crystallized under constrained conditions. Some other authors [28, 32] have evidenced a clear confinement effect of the amorphous phase appearing during primary crystallization, inducing RAF

formation, T_g increase and enhanced dynamic fragility around T_g. For example, Delpouve et al. [24, 33, 34], using the concept of Cooperative Rearranging Regions (CRR), originally introduced by Adam and Gibbs [35], and, following Donth's approach [36], evidenced a confining effect due to the crystallization inducing a drastic reduction in the characteristic length of this CRR. Still, in such semi-crystalline systems, it is difficult to decorrelate the pure geometrical confinement from the coupling between the amorphous and the crystalline phases and alternative ways of confinement have to be used.

Some authors measured the T_g variation by ellipsometry of spincoated PLLA thin films on different substrates. While Narladkar et al. [37] observed a decrease of the T_g for film thicknesses below 50 nm on non-interacting surface, Spièce et al. [38] reported an increase of several degrees for two different substrates. Those contradictory results point out the importance of polymer-surface interactions and free surfaces that can be responsible for enhanced molecular mobility in thin film [39, 40]. Such free interfaces are suppressed when the thin polymer film is sandwiched between confining walls. The original layer-multiplying co-extrusion process allows creating multi-nanolayered systems in which one polymer is sandwiched between layers of another rigid confining polymer, creating capped symmetric interfaces. A further advantage is that those unique 'nanostructured bulk materials' can be characterized with conventional techniques for bulk materials. In conclusion, the nanolayer co-extrusion process is an interesting means for mimicking symmetric polymer confinement between hard walls in controlling geometrical constraints.

In our study, nanolayer co-extrusion has been used for the first time to confine PLA. Polystyrene (PS) is chosen as confining polymer since it provides non-interacting surface towards PLA and its T_g (around 100°C) allows for a post-annealing treatment at 85°C inducing PLA cold crystallization under confinement. The study of amorphous and crystallized PLA/PS nanolayered films should shed additional light above the macromolecular mobility in the amorphous phase and the coupling between the amorphous and crystalline phases in PLA under geometrical confinement.

2. Experimental

2.1. Process and crystallization parameters

Polylactide (PLLA) pellets were purchased from Corbion Purac (PLA REVODE 190). The content of *L,L*-lactide was higher than 99 mol-%. The mass average molar mass, measured by GPC (Agilent 220 HT) using PS standards, was M_w = 177 kg.mol^{-1} and the dispersity Đ, defined as M_w/M_n, was 1.64. The gyration radius, estimated from the plot of Fang et al. [41], was around 20 nm. Polystyrene (PS) pellets were obtained from Total Petrochemicals (PS 1340).

The layer-multiplying co-extrusion process was used to fabricate multi-layered films of 3, 513 and 2049 alternating layers of PLLA and PS. The process is presented in the *Figure 1*. It consists in two single screw extruders of 20 mm with gear pumps, a three-layer feed block (A-B-A), a series of layer-multiplying elements, a flat die and chill rolls. The weight percentage of PLLA in the multilayer film is 25 %. The initial three-layer (PS/PLLA/PS) polymer flow enters a mixing section, followed by a sequence of layer-multiplying elements. The principle of the layer-multiplying elements is to cut the flow in half vertically, and to superpose, compress and stretch it to its original width, hence doubling the number of layers with each element. A series of n elements leads thus to $2^{n+1}+1$ alternating layers. The extrusion conditions are given in Supporting Information (SI 1).

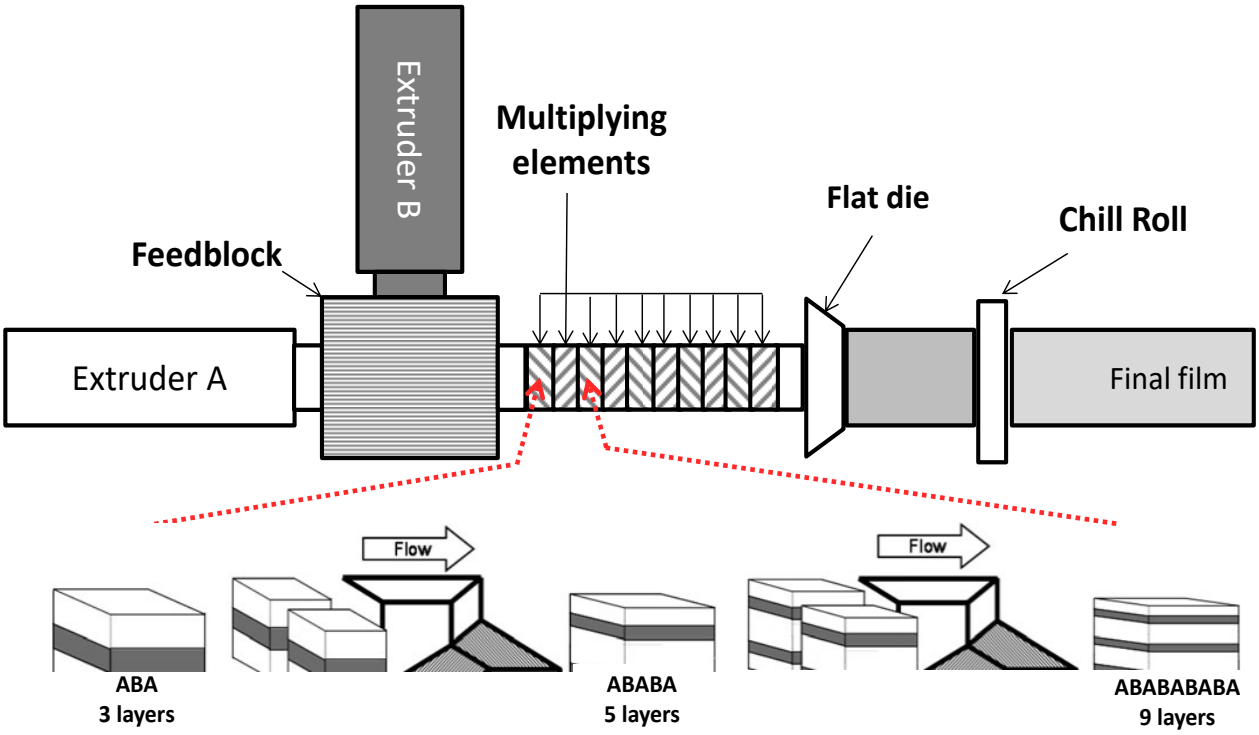

Figure 1. Principle of the layer-multiplying co-extrusion process

The set of samples, presented in *Table 1*, consisted of a blank sample, being the initial three-layer coextruded film with an individual PLLA layer thickness of 30000 nm, an intermediate sample (PLLA layer thickness of 300 nm), and one confined sample (20 nm). The latter PLLA layer thickness is in the order of the gyration radius of PLLA. After extrusion, some films were sandwiched between two sheets of Teflon and two stainless steel plates, and annealed in a heating press (Gribite) during 180 minutes at 85°C and a pressure set to 5 x 10^6 Pa.

Table 1. PS/PLLA multilayered films characteristics and process conditions.

Number of multiplying elements	Number of layers	Total film thickness (µm)	Nominal PLLA layer thickness (nm)
0	3	120	30000
8	513	300	300
10	2049	80	20

2.2. Characterization techniques

Melt rheology. The melt viscosities of PLLA and PS were measured using an Anton Paar MCR 502 rheometer in an oscillatory mode between 0.01 and 100 rad/s. The domain of linear strain was determined by performing preliminary deformation sweeps, and the working strain was set to 1% for both polymers. The shear viscosity as a function of shear rate was calculated using the Cox-Merz rule.

Atomic force microscopy (AFM). AFM was used to characterize the layered morphology of the coextruded films. AFM images were obtained in tapping mode using a multimode microscope controlled by a Veeco Nanoscope V controller. The tips (silicon, spring constant 40 N/m, oscillation frequency ca. 300 kHz) had a radius of curvature less than 10 nm. Specimens were taken from the center of the extruded films and were cut from the cross section with an ultramicrotome 2088 Ultrotome V (LKB) equipped with a diamond knife at a cutting speed of 1 mm/s. 15 images were recorded at full resolution (4096 × 4096 pixels), with a scan rate of 0.9 Hz, throughout the thickness of the film. Following the method developed by Bironeau et al. [42], the analysis of these 15 images containing each around 20 layers is representative of the whole sample with an uncertainty of 10%.

Wide Angle X-Ray Scattering (WAXS). WAXS experiments were performed using a Genix microsource (XENOCS) equipment operating at 50 kV and 1 mA. The Cu-Kα radiation used was selected with a curved mirror monochromator. The 2D patterns were recorded on a CCD camera from Photonic Science and the working distance was calibrated using a PLA sample. Integrated intensity profiles were computed from the 2D patterns using the FIT2D software. Before analysis standard corrections were applied to the patterns such as dark current substraction and background correction.Analyzes of the isothermal crystallization kinetics were made using the same X-ray generator and heating in situ the sample using a Linkam heating stage.

Modulated Temperature Differential Scanning Calorimetry (MT-DSC). The MT-DSC analyses were performed on a Thermal Analysis® Instrument DSC Q100. Nitrogen was used as purge gas (50 mL/min). The samples weights were about 5-10 mg, encapsulated in Tzero hermetic aluminum pans. Calibration in temperature and enthalpy was carried out using an indium standard. The specific heat capacity of each sample was measured using sapphire as a reference. The glass transition region of PLLA was analyzed using a heat-cool temperature modulation (oscillation amplitude of 3 K, oscillation period of 120 s, and heating rate of 1 K min^{-1}). The crystallization and melting of PLLA were analyzed using a heat-only temperature modulation (oscillation amplitude of 0.32 K, oscillation period of 60 s, and heating rate of 2 K min^{-1}). By MT-DSC, in addition of the modulated heat flow, the apparent specific complex heat capacity C* is obtained from the complete deconvolution procedure proposed by Reading and co-authors [43]. Its in-phase component (C') versus temperature appears as a step, when its out-of-phase component (C'') represents a peak in the glass transition region.

3. Results and discussion

3.1. Optimization of the layer multiplying co-extrusion process

Both uniformity and continuity of the layers depend strongly on the viscosity ratio ρ between the two polymers, a viscosity ratio far from one can indeed result in phenomena of encapsulation of the polymer of high viscosity by the polymer of lower viscosity [44]. It is defined as follows:

$$\rho = \frac{\eta_{confined}}{\eta_{confining}}, \quad (1)$$

where $\eta_{confined}$ and $\eta_{confining}$ are respectively the viscosities of the confined polymer (in our case PLLA) and confining polymer (PS). The viscosity curves (available in the SI 2) show that in the shear rate range of the co-extrusion process, typically between 1 and 50 s^{-1}, the viscosity ratio was close to 1, which ensures homogeneity of the stratified flow and prevents from layer rupture when decreasing layer thickness [45].

Figure 2 depicts the AFM phase images obtained on as-extruded and annealed films. A reasonable contrast between the two components (PS corresponds to the larger layers) enabled to reveal the layered structure and to perform image analysis in order to measure a thickness distribution of the layers.

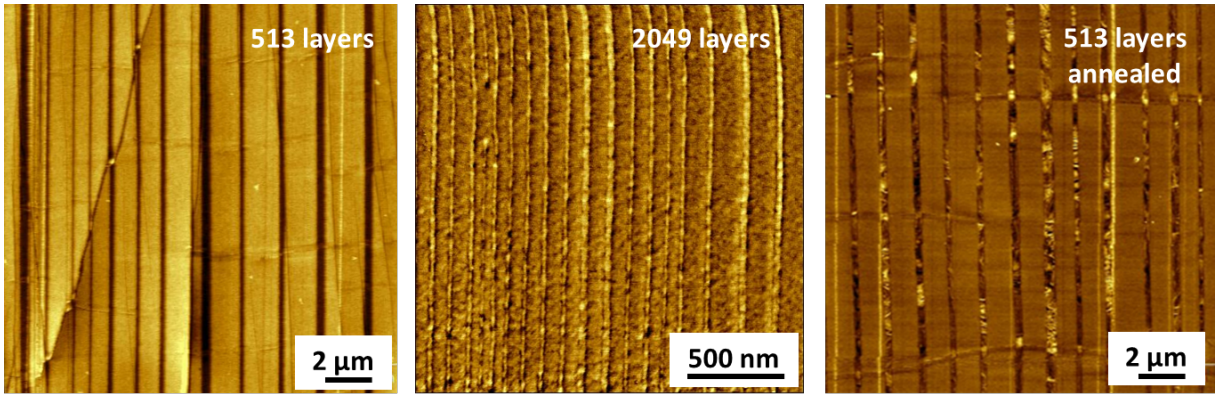

Figure 2. Tapping mode AFM phase images of nanolayered PS/PLLA containing different number of layers as indicated.

The AFM images showed continuous and relatively uniform layers of PS and PLLA. Furthermore it can be observed that the layer continuity was maintained after crystallization. The observed distributions of thickness of PLLA layers for each sample are given in *Figures 3a* (2049 layers) and *3b* (513 layers). The distribution of thickness can be represented by a log-normal distribution. The average layer thicknesses of PLLA was 220 ± 50 nm for the films containing 513 layers and 20 ± 5 nm for the films with 2049 layers, which was in reasonable agreement with the expected nominal thickness given in *Table 2*.

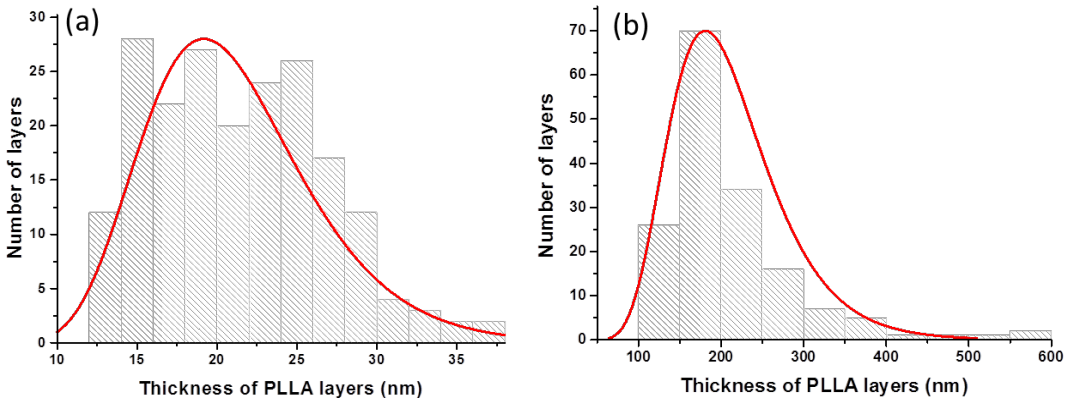

Figure 3. Distributions of PLLA layer thickness for the films containing 2049 layers (a) and 513 layers (b). The red lines represent the log-normal distribution curves.

3.2. Crystallization of PLLA under confinement

Figure 4a shows the WAXS patterns obtained on as-extruded PS/PLLA films. Only the amorphous halos of PLLA and PS were visible, indicating that PLLA was amorphous after the extrusion, which was expected because of the slow crystallization kinetics of PLLA [46, 47]. The temperature window between the T_gs of PLLA (60°C) and PS (100°C) allowed for isothermal cold-crystallization of PLLA under hard confinement, *i.e.* between two glassy polymer walls. The DSC curves of the films annealed at 85 °C for 3 h (given in SI 3) did not exhibit any cold crystallization peak, indicating that the crystallization after 3 hours was complete for all the samples. *Figure 4b* shows the WAXS diffractograms of annealed PLLA. The strong reflections of PLLA at 2θ around 16.4° and 2θ = 18.5°, attributed to the 200/110 and 203 planes respectively, could be observed for all samples [48, 49]. The present crystallization temperature (85 °C) would theoretically favor the α'-polymorph of PLLA [26, 50]. However the minor reflections characteristic of the α'-polymorph could not be observed here, most probably because of the sensitivity limit of the DRX measurement as PLLA accounts only for 25 wt% of the sample. As a consequence, the occurrence of the α'-polymorph cannot be asserted.

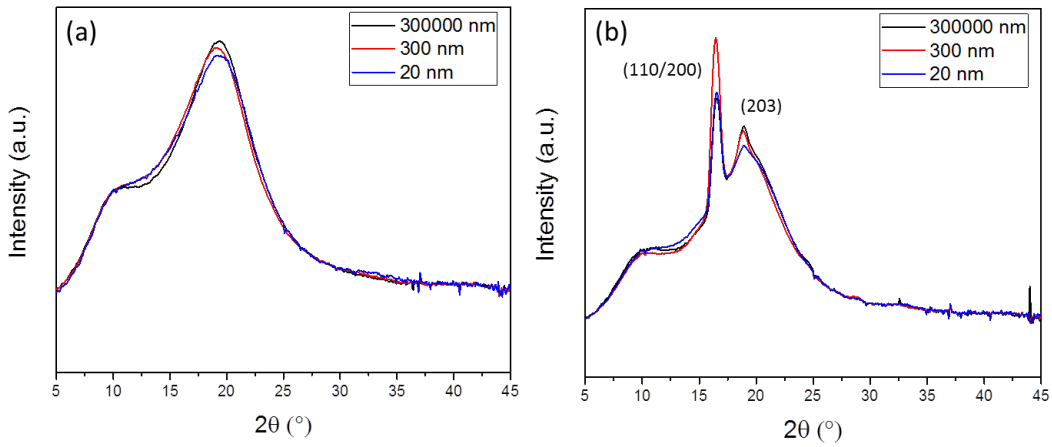

Figure 4. WAXS intensity profiles of PS/PLLA films (a) before annealing (b) after annealing at 85°C during 180 minutes.

In the aim to study the impact of the confinement on the crystallization kinetics of PLLA, the relative crystallinity of PLLA was recorded by WAXS during isothermal annealing at 85 °C for different layer thicknesses. For this experiment, several films were stacked in order to increase the WAXS signal, introduced in a heating stage and heated from the bottom side. Therefore, the temperature control in the sample thickness was not as efficient as it can be expected in the heating press. The results, shown in the *Figure 5*, are thus used for the sake of comparison of crystallization kinetics under these conditions.

The isothermal crystallization kinetics of PLLA was analyzed with the help of the Avrami equation:

$$\alpha(t) = 1 - \exp(-K \cdot t^n), \qquad (2)$$

where α(t) is the relative crystallinity fraction at time t, K is the crystallization rate constant and n is the Avrami exponent depending on the nucleation and the growth geometry (sphere, disc, etc.) [51]. Equation (2) can be transformed into the following form:

$$\ln(-\ln(1-\alpha(t))) = n\ln(t) + \ln K, \qquad (3)$$

The kinetic parameters n and K can therefore be obtained by plotting ln(-ln(1-α(t))) as a function of ln(t). The Avrami model in *Figure 5a,* for 30000 nm sample, fitted well with experiments for relative crystallinity below 0.8, with an Avrami exponent close to 3, associated according to the Avrami theory [51], with a three dimensional crystallization growth with an instantaneous nucleation. However, for higher relative crystallinity (above 0.8), the experimental curve showed a slower crystallization than the one predicted by the Avrami model, which is typical for the occurrence of a secondary crystallization. The non-linear behavior for the double logarithm of the relative crystallinity in *Figure 5b* is another signature of this secondary crystallization. For 20 and 300 nm samples, this secondary crystallization is suppressed and the Avrami model fits perfectly with experiments, which corresponds to linear curves for the double logarithm of the relative crystallinity in *Figure 5b*. The Avrami exponents, n=1.7 and 1.6 for individual PLLA layer thicknesses of 20 nm and 300 nm respectively (*Table 2*), correspond to a two dimensional crystallization growth with an instantaneous nucleation. The crystallization rate (K) and crystallization half-time ($t_{1/2}$) are given in *Table 2*. We observed a decrease in K when PLLA thickness decreases correlated with the increase in $t_{1/2}$. The delay of the overall crystallization rate as the layer thickness decreases was already observed for other polymers in multi-nanolayered systems, such as PEO [52] or PET [53].

To summarize, in the thin layers the crystallization rate was reduced, the crystalline growth was restricted to two dimensions and the secondary crystallization was not observed.

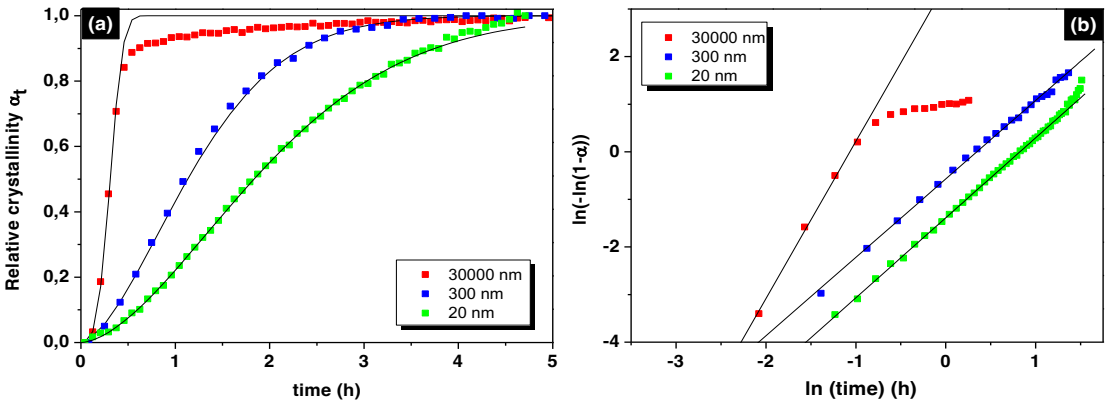

Figure 5. Relative crystallization and Avrami plots versus time for 30000 nm, 300 nm and 20 nm isothermal crystallization at 85°C (a); Double logarithm versus ln(time) and the Avrami plots (black lines) for annealed samples (30000 nm, 300 nm and 20 nm) at 85°C (b).

3.3. Three-phase model of confined PLLA

As previously mentioned, PLLA can be described by a three-phase model and the quantification of each fraction is possible from calorimetric analysis. The degree of crystallinity (X_c) of the PLA samples was calculated from

$$X_c = \frac{\Delta H_m - \Delta H_{cc}}{\Delta H_m^0}, \qquad (4)$$

where ΔH_m is the enthalpy of melting after subtraction of the small exothermal event at the beginning of the melting peak, ΔH_{cc} is the cold crystallization enthalpy (both ΔH_m and ΔH_{cc} are normalized to PLLA content), and ΔH_m^0 is the standard melting enthalpy, *i.e.* melting enthalpy of the perfect crystal of infinite size (93.1 J/g) [54]. The use of MT-DSC is specifically required in the present study as the glass transition of PS occurs in the same temperature range as the cold crystallization of PLLA. An example of the analysis procedure is given in Supporting Information (SI 4). The difference between the cold crystallization enthalpy and the melting enthalpy for the determination of the degree of crystallinity was double checked using the average heat flow signal which equals the classical DSC signal, and the reversing and the non-reversing heat flow signals from MT-DSC. The content of the RAF, $X_{RA,}$ can be calculated from:

$$X_c + X_{MA} + X_{RA} = 100\% \text{ with } X_{MA} = \frac{\Delta C_p}{\Delta C_p^0}, \qquad (5)$$

where X_{MA} is the content of MAF, ΔC_p is the heat capacity change measured at the glass transition and ΔC_p^0 the heat capacity change of the fully amorphous sample. The value of ΔC_p^0 was measured using the rejuvenated initial films. The numerical results are presented in *Table 2*. The crystallinity degree of PLLA after annealing increased with the decrease of the layer thickness. The underlying physics are not yet established, but different types of behaviour were already observed. Mackey et al. [55] showed a slight decrease in crystallinity for confined polyvinylidene fluoride (PVDF), while Wang et al. [56] did

not observe any difference in crystallinity for confined poly(ethylene oxide) (PEO). Our result is comparable to the one of Boufarguine et al. [57] for the couple PLA/PHBV. They observed an increase of the crystallinity degree for PHBV when the polymer was confined in thin layers, possibly attributed to the strong molecular orientation induced by the polymer flow in the multiplying elements or the development of crystalline orientations. In conclusion, the confinement retarded the kinetics of crystallization but allowed reaching a higher degree of crystallinity without secondary crystallization.

The RAF of PLLA decreased from about 40 to 10% as the layer thickness was reduced from 30000 to 300 nm, and it was not observed after 3h crystallization in confined PLLA layers of 20 nm thickness, although those samples had the highest degree of crystallinity (*Table 2*). For those films, a 25% content of RAF was recorded after a long annealing time (after 9h). This means that the decoupling between crystalline and amorphous phases was possible in thin layers (for 3h thermal annealing). Several hypotheses can be suggested to explain this result. First, it might be associated to a pure geometric constraint effect. It has been proposed that the domain of molecular segments involved in the coupling should reach a critical length to produce an intermediate phase [21]. In a layer of 20 nm, the amorphous phase is besides strongly confined by the few existing crystalline lamellae that contribute to the further decrease of the available space. The change in the crystalline growth from a three dimensional to a two dimensional order, as deduced from the Avrami equation, was thus considered as a possible cause favouring the decoupling.

Another hypothesis is that the modification of the crystallization kinetics in thin layers delayed the formation of the RAF. In a previous work, it was reported that prolonging the annealing time favoured the gradual conversion of MAF into RAF with time [25]. The decoupling of the amorphous and the crystalline phase in the confined configuration and the absence of secondary crystallization had thus an effect of retard on the formation of the RAF, the quantity of which even after 9 h of annealing is still smaller than that of 3 h of annealing of bulk PLLA (*Table 2*).

Table 2. Structural and thermal parameters of PLLA confined at different thickness obtained from in-situ WAXS and MT-DSC heat-only analyses.

PLLA nominal thickness	$t_{1/2}$ (h)	n	K (h^{-n})	ΔC_p^0 ($Jg^{-1}K^{-1}$)	ΔC_p ($Jg^{-1}K^{-1}$)	X_c (%)	X_{MA} (%)	X_{RA} (%)
30000 nm*	0.31	3.3	33.52	0.48±0.02	0.16±0.02	28±2	33±6	39±8
300 nm*	1.13	1.6	0.57	0.44±0.02	0.20±0.02	36±2	45±6	19±8
20 nm*	1.84	1.7	0.25	0.44±0.02	0.25±0.02	43±2	57±7	0±9
20 nm**				0.44±0.02	0.13±0.02	45±2	30±6	25±8

Annealing conditions: *85 °C during 3h **85°C during 9 h
$t_{1/2}$ crystallization half-time
n Avrami exponent
K crystallization rate constant
ΔC_p^0 heat capacity step of PLLA with a nil crystallinity degree
ΔC_p heat capacity step of annealed PLLA
X_c crystallinity degree
X_{MA} content of the mobile amorphous fraction (MAF)
X_{RA} content of the rigid amorphous fraction (RAF)

To summarize, contrary to what was observed for bulk samples, the crystalline phase development under confinement occurred without simultaneous creation of RAF and secondary crystallization. The RAF was created at longer times with sufficient delay to allow the tuning of the content of RAF at high crystallinity degrees. The confined samples obtained after 3h annealing at 85°C offer a unique combination with maximal degree of crystallinity and no RAF at all, presenting a complete decoupling between amorphous and crystalline phases.

3.4. Dynamic heterogeneity of confined PLLA

The mobility landscape of the amorphous phase can be pictured by the size of the cooperative rearranging regions (CRR) that is impacted by structural constraints. As mentioned in the introduction, the decrease of the CRR size has been commonly reported in semi-crystalline polymers [33, 58], revealing a restriction in amorphous chain segment mobility due to the presence of crystalline phase. However, in these systems, the strong interfacial interactions between crystalline and amorphous phases make it difficult to determine the exact nature of these constraints. Initially pure geometrical confinement was invoked to explain the disturbance of the amorphous phase dynamics [58], but more recently the possibility of an additional alteration of dynamics induced by the RAF has been suggested [24]. It is nevertheless difficult to discriminate between the effects of the geometrical confinement and the "covalent coupling" of the amorphous phase to crystalline domains, corresponding to RAF. In this context, the samples obtained via nanolayer coextrusion in which PLLA is confined in thin layers of 20 nm and crystallized at its maximum value, in presence of RAF (25% when annealed 9 hours) or not (0% when annealed 3 hours), offer unique opportunity to gain insight in the impact of geometrical confinement and RAF on the dynamic landscape of the amorphous phase.

The size of the CRR can be calculated directly from MT-DSC measurements using Donth's approach [36, 59]. An example of how to retrieve the required physical quantities is shown in Supporting Information (SI 5). The cooperativity volume $\xi_{T\alpha}^{\ 3}$ of a CRR at the dynamic glass transition temperature T_α can be estimated from the equation below:

$$\xi_{T\alpha}^3 = \frac{\left(1/C_p\right)_{Glass\ T\alpha} - \left(1/C_p\right)_{Liquid\ T\alpha}}{\rho\left(\delta T\right)^2} k_B T_\alpha^2, \qquad (6)$$

where k_B is the Boltzmann constant, δT the average temperature fluctuation related to the dynamic glass transition of a CRR, ρ the density equal to 1.25 g.cm^{-3} for the amorphous phase of PLLA, and C_p the specific heat capacity at constant pressure. When applying the fluctuation-dissipation theorem (FDT) and fitting the out-of-phase component C''(T) or the derivative of C'(T) with respect to temperature with a Gaussian (supposing temperature variable and frequency constant), δT corresponds to the standard deviation of this Gaussian [59], and T_α corresponds to its maximum. The values of $C_{p\ glass\ T\alpha}$ and $C_{p\ liquid\ T\alpha}$ are obtained from the C' signal by prolonging the glass and liquid lines to the dynamic glass transition temperature after normalization to the quantity relaxing at the glass transition, *i.e.* the MAF content.

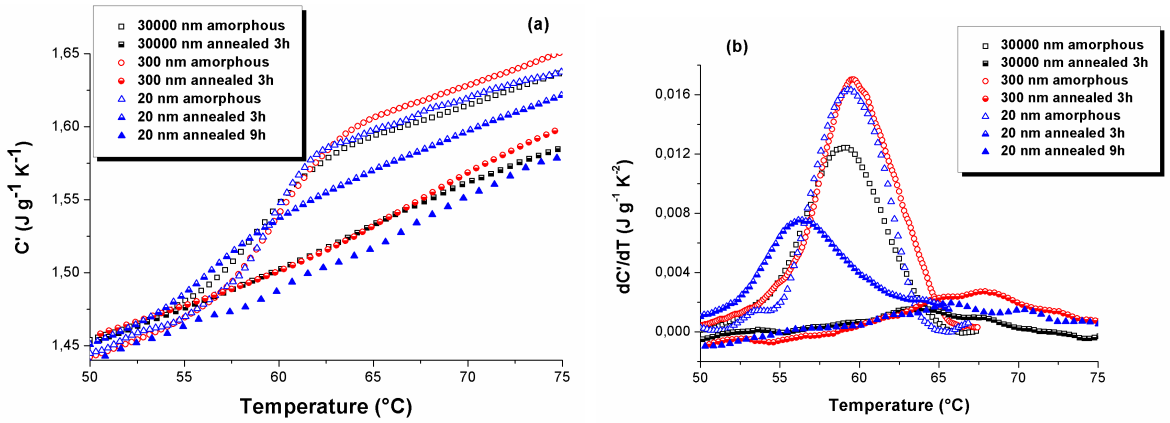

Figure 6. Temperature dependence of (a) real part (C') (b) imaginary part (C'') of complex heat capacity (C) for different multilayered PS/PLLA films when PLLA is amorphous or crystallized.*

The real part and imaginary part of the complex heat capacity during the glass transition of PLLA are presented in *Figure 6*. The curves are plotted before any normalization; however the C' curves have been shifted for the consistency of Cp_{glass} with the computed values linked to the vibrational molecular motions, as recommended by Pyda et al. [60]. For the thick layers (30000 and 300 nm), the increase of the crystallinity degree (X_c) of annealed PLLA layers caused the decrease of the amplitude of the heat capacity change because less amorphous phase was involved in the relaxation (*Figure 6a*). Besides, a shift of the glass transition to higher temperatures was observed due to the constraints generated by the crystalline environment, which caused the amorphous phase of bulk polymers to require more thermal energy for relaxation in the presence of crystallites. The T_α shift was concomitant with the presence of crystals and RAF [28]. Moreover the glass transition domain was significantly broadened, meaning that δT strongly increased and that the peak of C" almost disappeared (*Figure 6b*). The same effect was observed in thin layers (20 nm) after 9 h of annealing, when 25% RAF was generated. However, the behaviour of PLLA after 3h annealing in the 20 nm layers was quite different. Due to the absence of RAF, the heat capacity step at the glass transition was in between the other semi-crystalline PLLA and the amorphous ones (*Figure 6a*). The C'' peak was furthermore perfectly discernible (*Figure 6b*). Finally, in comparison to the 20 nm amorphous PLLA, T_α did not shift to higher temperatures but 3°C below, and δT was only slightly higher.

The quantification of the changes in the dynamic heterogeneity of PLLA layers under increasing confinement is given in *Table 3*, presenting the variation of the dynamic glass transition temperature (T_α), the mean temperature fluctuation, and the cooperativity length for both amorphous (as-extruded films) and crystallized (annealed films) PLLA. No impact of the layer thickness on the T_α of amorphous PLLA samples was observed, which is in contradiction with the results of Narladkar et al. [37] and Spièce et al. [38]. To explain these results, one might suggest that in the absence of free surfaces in multi-nanolayered films, there was no change of the local free volume at the interface. Only a slight shift of 3°C towards low temperatures was observed for 20 nm PLLA after 3h annealing. In this sample, the confinement of the PLLA amorphous phase was stronger, although not quantified, since it was caused by both the layers of glassy PS and the crystallites. Attributing or not this decrease of T_α to a confinement effect is questionable. By contrast, the shift of T_α to higher temperatures recorded for the other semi-crystalline PLLA was clearly correlated with the apparition of RAF. This is coherent with earlier works that report that the T_α of PLA increases significantly when annealing conditions favoring strong coupling [61].

Table 3. Quantification of the changes in the dynamic heterogeneity of PLLA layers for different layer thickness and annealing time.

PLLA nominal thickness	X_{RA} (%)	T_α (°C)	δT (°C)	$\xi_{T\alpha}$ (nm)
30000 nm	0	59.0±0.5	3.0±0.2	2.9±0.3
30000 nm*	39	65.5±0.5	5.3±0.2	2.0±0.2
300 nm	0	59.5±0.5	2.8±0.2	3.0±0.3
300 nm*	9	67.5±0.5	5.6±0.2	1.9±0.2
20 nm	0	59.5±0.5	2.8±0.2	3.0±0.3
20 nm*	0	56.5±0.5	3.1±0.2	2.7±0.3
20 nm**	30	67.5±0.5	7.5±0.2	1.6±0.2

*Crystallized PLLA with annealing conditions: 85 °C during 3h, **85°C during 9 h

For all amorphous PLLA samples, the cooperativity length was close to three nanometers. Contrary to what was observed on other amorphous polymers (poly(methyl methacrylate), polycarbonate, PS) [62-64], the cooperativity length in amorphous PLLA did not decrease when the PLLA layer thickness was reduced. This result is consistent with the absence of variations in T_α. As mentioned above, the effects of confinement were less easily apparent in these systems, even for layers as thin as 20 nm.

After 3h annealing, the 20 nm PLLA exhibited a cooperativity length around 2.7 nm. In this material there was no RAF, thus no interfacial area of coupling between amorphous zones and crystals. Moreover, due to the low compatibility of PLLA and PS, PS surfaces behaved as “slippery surfaces” and did not impose any supplementary restrictions. As a consequence, it is deduced that the pure geometric restrictions imposed by the neighboring layers of PS and the crystallites poorly impacted the dynamic heterogeneity in PLLA.

On the contrary, in all semi-crystalline PLLA exhibiting substantial contents of RAF, the cooperativity length decreased significantly, down to values ranging from 1.6 to 2.0 nm. Esposito et al. [65] reported from MT-DSC and dielectric spectroscopy measurements that the width of the glass transition in semi-crystalline materials was strongly related to the level of coupling between amorphous and crystalline phases. If the level of coupling is high, the structural constraints generated by the crystalline phase progressively transfer to the non-crystalline part of the material. This leads to a mobility gradient in the amorphous phase, the signature of which is a broad distribution of relaxation temperatures and therefore a significantly reduced CRR size.

To give a summary, the crystallization of PLLA under geometrical confinement offered favorable conditions for the decoupling of the amorphous and crystalline phases, characterized by the decrease of the coupled phase (RAF quantity). Consequently, the impact of crystallization on the relaxation phenomena in the amorphous phase was unique, leading to an almost negligible decrease of the glass

transition and reduction of the cooperativity length. In that case, the CRR size became independent from the degree of crystallinity of the samples. In bulk materials, where the crystal growth adds a supplementary constraint to the geometric confinement effect because one macromolecule is part of both the confining and the confined part, an usual increase of both the dynamic glass transition and the dynamic heterogeneity was recorded. In the mobility landscape of semi-crystalline polymers, the role of the RAF is thus crucial since the volume of the MAF involved in the relaxation processes depends on its degree of decoupling from the crystal. Consequently, even in the confined space, the increase of the RAF quantity with time reduced significantly the CRR size (*Table 3*).

4. Conclusion

While RAF is usually known to form concomitantly with crystallization for bulk PLLA, a complete decorrelation between these two phenomena has been observed in PLLA confined in nanolayered PLLA/PS films, fabricated with the layer multiplying co-extrusion process. This allowed to rationally control the quantity of created RAF and to fabricate unique samples with nanoconfined PLLA, crystallized at its maximum value and without any RAF content. Moreover, comparing samples of geometrically confined PLLA presenting different contents of RAF, allowed to discriminate the effects of confinement and coupling on the dynamic landscape of the amorphous phase. We observed that geometrical confinement impacted barely the amorphous dynamics, while phase coupling had a major influence on the dynamic heterogeneity and increased the alpha transition temperature. This knowledge can offer a novel strategy to optimize semi-crystalline polymers' performance properties that are impacted by the presence of rigid amorphous phases.

References

1. Jackson, C.L. and G.B. McKenna, *The glass transition of organic liquids confined to small pores.* Journal of Non-Crystalline Solids, 1991. **131**: p. 221-224.
2. Alcoutlabi, M. and G.B. McKenna, *Effects of confinement on material behaviour at the nanometre size scale.* Journal of Physics: Condensed Matter, 2005. **17**(15): p. R461.
3. Forrest, J.A. and K. Dalnoki-Veress, *The glass transition in thin polymer films.* Advances in Colloid and Interface Science, 2001. **94**(1): p. 167-195.
4. Kremer, F., M. Tress, and E.U. Mapesa, *Glassy dynamics and glass transition in nanometric layers and films: A silver lining on the horizon.* Journal of Non-Crystalline Solids, 2015. **407**: p. 277-283.
5. Michell, R.M. and A.J. Müller, *Confined crystallization of polymeric materials.* Progress in Polymer Science, 2016. **54**: p. 183-213.
6. Prud'homme, R.E., *Crystallization and morphology of ultrathin films of homopolymers and polymer blends.* Progress in Polymer Science, 2016. **54**: p. 214-231.
7. Massa, M.V. and K. Dalnoki-Veress, *Homogeneous crystallization of poly (ethylene oxide) confined to droplets: the dependence of the crystal nucleation rate on length scale and temperature.* Physical review letters, 2004. **92**(25): p. 255509.
8. Forrest, J., K. Dalnoki-Veress, and J. Dutcher, *Interface and chain confinement effects on the glass transition temperature of thin polymer films.* Physical Review E, 1997. **56**(5): p. 5705.
9. Carr, J.M., et al., *Confined crystallization in polymer nanolayered films: A review.* Journal of Materials Research, 2012. **27**(10): p. 1326-1350.
10. Jackson, C.L. and G.B. McKenna, *Vitrification and crystallization of organic liquids confined to nanoscale pores.* Chemistry of Materials, 1996. **8**(8): p. 2128-2137.
11. Michell, R.M., et al., *Confined crystallization of polymers within anodic aluminum oxide templates.* Journal of Polymer Science Part B: Polymer Physics, 2014. **52**(18): p. 1179-1194.
12. Wang, B. and S. Krause, *Properties of dimethylsiloxane microphases in phase-separated dimethylsiloxane block copolymers.* Macromolecules, 1987. **20**(9): p. 2201-2208.
13. Wang, T., et al., *Confined growth of poly (butylene succinate) in its miscible blends with poly (vinylidene fluoride): morphology and growth kinetics.* The Journal of Physical Chemistry B, 2011. **115**(24): p. 7814-7822.
14. Huang, H.-D., et al., *Poly (L-lactic acid) crystallization in a confined space containing graphene oxide nanosheets.* The Journal of Physical Chemistry B, 2013. **117**(36): p. 10641-10651.
15. Aharoni, S.M., *Increased glass transition temperature in motionally constrained semicrystalline polymers.* Polymers for Advanced Technologies, 1998. **9**(3): p. 169-201.
16. Schick, C., A. Wurm, and A. Mohammed, *Formation and disappearance of the rigid amorphous fraction in semicrystalline polymers revealed from frequency dependent heat capacity.* Thermochimica Acta, 2003. **396**(1): p. 119-132.
17. Wunderlich, B., *Reversible crystallization and the rigid–amorphous phase in semicrystalline macromolecules.* Progress in Polymer Science, 2003. **28**(3): p. 383-450.
18. Kolesov, I. and R. Androsch, *The rigid amorphous fraction of cold-crystallized polyamide 6.* Polymer, 2012. **53**(21): p. 4770-4777.
19. Rastogi, R., et al., *The three-phase structure and mechanical properties of poly(ethylene terephthalate).* Journal of Polymer Science Part B: Polymer Physics, 2004. **42**(11): p. 2092-2106.
20. Hu, Y., et al., *Oxygen transport and free volume in cold-crystallized and melt-crystallized poly (ethylene naphthalate).* Macromolecules, 2002. **35**(19): p. 7326-7337.

21. Lin, J., S. Shenogin, and S. Nazarenko, *Oxygen solubility and specific volume of rigid amorphous fraction in semicrystalline poly(ethylene terephthalate).* Polymer, 2002. **43**(17): p. 4733-4743.
22. Pan, P. and Y. Inoue, *Polymorphism and isomorphism in biodegradable polyesters.* Progress in Polymer Science, 2009. **34**(7): p. 605-640.
23. Del Rio, J., et al., *A PALS contribution to the supramolecular structure of poly (L-lactide).* Macromolecules, 2010. **43**(10): p. 4698-4707.
24. Delpouve, N., A. Saiter, and E. Dargent, *Cooperativity length evolution during crystallization of poly (lactic acid).* European Polymer Journal, 2011. **47**(12): p. 2414-2423.
25. Fernandes-Nassar, S., et al., *Multi-scale analysis of the impact of polylactide morphology on gas barrier properties.* Polymer, 2017. **108**: p. 163-172.
26. Guinault, A., et al., *Impact of crystallinity of poly (lactide) on helium and oxygen barrier properties.* European Polymer Journal, 2012. **48**(4): p. 779-788.
27. Righetti, M.C., D. Prevosto, and E. Tombari, *Time and temperature evolution of the rigid amorphous fraction and differently constrained amorphous fractions in PLLA.* Macromolecular Chemistry and Physics, 2016. **217**(18): p. 2013-2026.
28. Zuza, E., et al., *Glass transition behavior and dynamic fragility in polylactides containing mobile and rigid amorphous fractions.* Polymer, 2008. **49**(20): p. 4427-4432.
29. Righetti, M.C. and E. Tombari, *Crystalline, mobile amorphous and rigid amorphous fractions in poly (L-lactic acid) by TMDSC.* Thermochimica acta, 2011. **522**(1): p. 118-127.
30. Mijovic, J., M. Sun, and Y. Han, *Normal and segmental mode dynamics of end-functionalized poly (propylene oxide) by dielectric relaxation spectroscopy and dynamic mechanical spectroscopy.* Macromolecules, 2002. **35**(16): p. 6417-6425.
31. Fitz, B.D., D.D. Jamiolkowski, and S. Andjelić, *T g Depression in poly (l (−)-lactide) crystallized under partially constrained conditions.* Macromolecules, 2002. **35**(15): p. 5869-5872.
32. Brás, A.R., et al., *Crystallization of poly (L-lactic acid) probed with dielectric relaxation spectroscopy.* Macromolecules, 2006. **39**(19): p. 6513-6520.
33. Delpouve, N., et al., *Cooperative rearranging region size in semi-crystalline poly (l-lactic acid).* Polymer, 2008. **49**(13): p. 3130-3135.
34. Saiter, A., et al., *Cooperative rearranging region size determination by temperature modulated DSC in semi-crystalline poly (L-lactide acid).* European Polymer Journal, 2007. **43**(11): p. 4675-4682.
35. Adam, G. and J.H. Gibbs, *On the temperature dependence of cooperative relaxation properties in glass-forming liquids.* The journal of chemical physics, 1965. **43**(1): p. 139-146.
36. Donth, E., *The size of cooperatively rearranging regions at the glass transition.* Journal of Non-Crystalline Solids, 1982. **53**(3): p. 325-330.
37. Narladkar, A., et al. *Difference in glass transition behavior between semi crystalline and amorphous poly (lactic acid) thin films*. in *Macromolecular symposia*. 2008. Wiley Online Library.
38. Spiece, J., et al., *Are polymers glassier upon confinement?* Soft Matter, 2015. **11**(31): p. 6179-6186.
39. Ediger, M. and J. Forrest, *Dynamics near free surfaces and the glass transition in thin polymer films: a view to the future.* Macromolecules, 2013. **47**(2): p. 471-478.
40. Fu, Y., et al., *Evidence of Enhanced Mobility at the Free Surface of Supported Polymer Films by in Situ Variable-Temperature Time-of-Flight-Secondary Ion Mass Spectrometry.* Analytical chemistry, 2013. **85**(22): p. 10725-10732.

41. Fang, H., et al., *Bimodal architecture and rheological and foaming properties for gamma-irradiated long-chain branched polylactides.* RSC Advances, 2013. **3**(23): p. 8783-8795.
42. Bironeau, A., et al., *Evaluation of morphological representative sample sizes for nanolayered polymer blends.* Journal of microscopy, 2016. **264**(1): p. 48-58.
43. Lacey, A., D. Price, and M. Reading, *Theory and practice of modulated temperature differential scanning calorimetry.* Modulated Temperature Differential Scanning Calorimetry, 2006: p. 1-81.
44. Ponting, M., A. Hiltner, and E. Baer. *Polymer nanostructures by forced assembly: process, structure, and properties*. in *Macromolecular symposia*. 2010. Wiley Online Library.
45. Bironeau, A., et al., *Existence of a critical layer thickness in PS/PMMA nanolayered films.* Macromolecules, 2017.
46. Courgneau, C., et al., *Effect of crystallization on barrier properties of formulated polylactide.* Polymer International, 2012. **61**(2): p. 180-189.
47. Saeidlou, S., et al., *Poly (lactic acid) crystallization.* Progress in Polymer Science, 2012. **37**(12): p. 1657-1677.
48. Stoclet, G., et al., *Thermal and strain-induced chain ordering in lactic acid stereocopolymers: influence of the composition in stereomers.* Macromolecules, 2011. **44**(12): p. 4961-4969.
49. Zhang, J., et al., *Disorder-to-order phase transition and multiple melting behavior of poly (L-lactide) investigated by simultaneous measurements of WAXD and DSC.* Macromolecules, 2008. **41**(4): p. 1352-1357.
50. Di Lorenzo, M.L., M. Cocca, and M. Malinconico, *Crystal polymorphism of poly (l-lactic acid) and its influence on thermal properties.* Thermochimica acta, 2011. **522**(1): p. 110-117.
51. Avrami, M., *Kinetics of phase change. I General theory.* The Journal of Chemical Physics, 1939. **7**(12): p. 1103-1112.
52. Wang, H., et al., *Crystallization kinetics of poly (ethylene oxide) in confined nanolayers.* Macromolecules, 2010. **43**(7): p. 3359-3364.
53. Flores, A., et al., *Confined crystallization of nanolayered poly (ethylene terephthalate) using X-ray diffraction methods.* Polymer, 2012. **53**(18): p. 3986-3993.
54. Fischer, E., H.J. Sterzel, and G. Wegner, *Investigation of the structure of solution grown crystals of lactide copolymers by means of chemical reactions.* Kolloid-Zeitschrift und Zeitschrift für Polymere, 1973. **251**(11): p. 980-990.
55. Mackey, M., et al., *Confined crystallization of PVDF and a PVDF-TFE copolymer in nanolayered films.* Journal of Polymer Science Part B: Polymer Physics, 2011. **49**(24): p. 1750-1761.
56. Wang, H., et al., *Confined crystallization of PEO in nanolayered films impacting structure and oxygen permeability.* Macromolecules, 2009. **42**(18): p. 7055-7066.
57. Boufarguine, M., et al., *PLA/PHBV films with improved mechanical and gas barrier properties.* Macromolecular Materials and Engineering, 2013. **298**(10): p. 1065-1073.
58. Schick, C. and E. Donth, *Characteristic length of glass transition: experimental evidence.* Physica Scripta, 1991. **43**(4): p. 423.
59. Hempel, E., et al., *Characteristic length of dynamic glass transition near T g for a wide assortment of glass-forming substances.* The Journal of Physical Chemistry B, 2000. **104**(11): p. 2460-2466.
60. Pyda, M., R. Bopp, and B. Wunderlich, *Heat capacity of poly (lactic acid).* The Journal of Chemical Thermodynamics, 2004. **36**(9): p. 731-742.
61. Saiter, A., et al., *Probing the chain segment mobility at the interface of semi-crystalline polylactide/clay nanocomposites.* European Polymer Journal, 2016. **78**: p. 274-289.

62. Arabeche, K., et al., *Study of the cooperativity at the glass transition temperature in PC/PMMA multilayered films: influence of thickness reduction from macro-to nanoscale.* Polymer, 2012. **53**(6): p. 1355-1361.
63. Tomczak, N., et al., *Segment dynamics in thin polystyrene films probed by single-molecule optics.* Journal of the American Chemical Society, 2004. **126**(15): p. 4748-4749.
64. Tran, T.A., S. Saïd, and Y. Grohens, *Nanoscale characteristic length at the glass transition in confined syndiotactic poly (methyl methacrylate).* Macromolecules, 2005. **38**(9): p. 3867-3871.
65. Esposito, A., et al., *From a Three-Phase Model to a Continuous Description of Molecular Mobility in Semicrystalline Poly (hydroxybutyrate-co-hydroxyvalerate).* Macromolecules, 2016. **49**(13): p. 4850-4861.